Current Research in Food Science 7 (2023) 100624

Contents lists available at ScienceDirect

Current Research in Food Science

journal homepage: www.sciencedirect.com/journal/current-research-in-food-science

Comparative evaluation of physical characteristics and volatile flavor components of *Bangia fusco-purpurea* subjected to hot air drying and vacuum freeze-drying

Jingna Wu [a,*], Nan Pan [b], Xiaoting Chen [b], Debiao Shan [a], Huifang Shi [a], Yingshan Qiu [a], Zhiyu Liu [b], Yongchang Su [b], Junfa Weng [c]

[a] *Xiamen Key Laboratory of Marine Medicinal Natural Products Resources, Fujian Universities and Colleges Engineering Research Center of Marine Biopharmaceutical Resources, Xiamen Medical College, 361023, Xiamen, PR China*
[b] *Fisheries Research Institute of Fujian, 361013, Xiamen, PR China*
[c] *Aquatic Science Research Institute of Putian, 351100, Putian, PR China*

ARTICLE INFO

Handling Editor: Professor Aiqian Ye

Keywords:
Bangia fusco-Purpurea
Microstructure
Rehydration capability
e-nose
GC×GC-TOF MS

ABSTRACT

Bangia fusco-purpurea is an economically important seaweed with Fujian characteristics. Given that its harvest is seasonal, drying is often used to remove moisture, extend storage time, and facilitate further processing. Hence, the current study sought to explore the impact of different drying processes on the quality and volatile fingerprints of *Bangia fusco-purpurea*. To this end, the effects of hot air drying (HAD) and vacuum freeze drying (VFD) on the drying characteristics, microstructure, rehydration, and volatile components of dried *B. fusco-purpurea* were investigated. The results showed that the water removal efficiency of HAD was significantly higher than that of VFD. However, VFD better preserved the skeletal structure of *B. fusco-purpurea* than HAD, with a faster rehydration rate and a more uniform cell structure after rehydration. Using electronic nose and comprehensive two-dimensional gas chromatography-time-of-flight mass spectrometry (GC × GC-TOF MS), significant differences in the volatile profiles of fresh, HAD, and VFD *B. fusco-purpurea* were assessed. E-nose analysis revealed that both HAD and VFD treatments significantly reduced sulfides, aromatic compounds, and nitrogen oxides in fresh *B. fusco-purpurea*. However, the alcohol, aldehyde, and ketone contents were lower in the VFD samples compared with HAD and fresh samples, whereas the content of methyl flavor substances was significantly higher. GC × GC-TOF MS analysis revealed that the most abundant volatile categories in HAD and VFD were hydrocarbons, alcohols, and esters. The number of volatile components in the HAD samples was significantly lower than in the VFD and fresh samples. As drying progressed, hydrocarbons and alcohols were formed in dried *B. fusco-purpurea* due to the thermal degradation of carbohydrates, lipids, amino acids, and the Maillard reaction. There were also significant flavor differences between HAD and VFD *B. fusco-purpurea*. Thus, although HAD exhibits better drying efficiency, VFD has more significant advantages in terms of product quality.

1. Introduction

Seaweeds are highly esteemed raw materials used in the food and medical industries due to their abundance of biologically active substances (Stévant et al., 2018). However, seaweed chemical composition is not fully understood when compared to that of land plants. Indeed, numerous factors significantly affect their composition, including the species, geographical location, maturity stage, and environmental conditions (Peña-Rodríguez et al., 2011). *Bangia fusco-purpurea* (Dillwyn) Lyngbye is a *Bangia* species member that belongs to the family Bangiaceae, order Bangiales, class Protoflorideophyceae, and phylum Rhodophyta. This species is primarily found in rocky intertidal zones, where it experiences significant variations in external salinity due to ebb and flow tides. Furthermore, it is subjected to extended periods of desiccation and prolonged exposure to high irradiance levels (J.N. Wu et al., 2021). *B. fusco-purpurea* contains significant quantities of proteins, fatty acids, and polysaccharides. In fact, the *B. fusco-purpurea* nutrient concentration surpasses that of *Porphyra* (Xu et al., 2022). Research conducted on the biological properties of metabolites derived from

* Corresponding author. Xiamen Key Laboratory of Marine Medicinal Natural Products Resources /Fujian Universities and Colleges Engineering Research Center of Marine Biopharmaceutical Resources, Xiamen Medical College, Xiamen, 361023, PR China.
E-mail address: wjn@xmmc.edu.cn (J. Wu).

https://doi.org/10.1016/j.crfs.2023.100624
Received 27 June 2023; Received in revised form 4 October 2023; Accepted 18 October 2023
Available online 20 October 2023

Abbreviations

e-nose	electronic nose
GC	gas chromatography
GC × GC-TOF MS	two-dimensional gas chromatography-time-of-flight mass spectrometry
VOC	volatile organic compound
HAD	hot air drying
HS	headspace
HS-SPME	headspace solid-phase microextraction
MR	moisture ratio
MS	mass spectrometry
PCA	principal component analysis
PUFAs	polyunsaturated fatty acids
RR	rehydration ratio
SEM	scanning electron microscopy
SPME	solid-phase microextraction
VFD	vacuum freeze-drying

B. fusco-purpurea has revealed various beneficial effects on human health, including antioxidant activity (Wu et al., 2015), pro-angiogenic (Jiang et al., 2021), anti-inflammatory (Zheng et al., 2022), and anti-tumor (Wu et al., 2021) properties.

A key challenge associated with utilizing seaweed in food and medicinal sectors is its seasonal harvest, which requires preservation and storage methods to ensure continuous year-round supply. Typically, seaweeds are harvested over a period of 2–3 months and subsequently processed in a systematic manner throughout the year (Obluchinskaya and Daurtseva, 2020). To facilitate their use in nutritional or industrial applications, fresh seaweeds are typically subjected to a drying process due to their substantial moisture content (ranging from 75% to 85%) and vulnerable character (Neoh et al., 2016). Various preservation techniques effectively prolong the seaweed lifespan, including conventional drying (López-Pérez et al., 2020). The dehydration process plays a vital role in eliminating a significant quantity of seaweed's aqueous content, leading to a decline in the water activity level. This effectively hinders microorganism proliferation while also diminishing the overall product bulk and mass. Such benefits have a favorable impact on storage and transportation expenses (Uribe et al., 2019). However, seaweed nutrient loss and structural deformation are natural consequences of the drying process (Stévant et al., 2018). Therefore, it is imperative to thoroughly investigate the impact of drying techniques on seaweed quality.

Sun drying is a prevalent and economical method. Nevertheless, the product quality may be impacted by weather and microbial intrusion and dust, insect, and bird contamination. Moreover, this process presents certain challenges regarding adequate quality control (Fudholi et al., 2014). Over time, artificial drying methods have become prevalent due to their controllable drying conditions, faster drying rates, and superior material quality as compared with non-artificial drying methods. Several drying technologies have been formulated, encompassing hot air drying (HAD), vacuum freeze-drying (VFD), infrared drying, and microwave drying (Ling et al., 2015). HAD utilizes hot air as the drying medium and relies on heat exchange through air convection to accomplish drying. Generally, heat-sensitive constituents, including bioactive components, undergo irreversible degradation or oxidation when subjected to prolonged, high-temperature dehydration procedures (Tan et al., 2021). The drying process can also modify the volatile organic compound (VOC) ratio in the product, including those with fruit and green aromas, including (E)-2-hexenal, hexanal and (E)-2-nonenal (Liu et al., 2022). VFD is currently considered the optimal approach for producing premium dried products. However, its disadvantages such as elevated production expenses, heightened energy consumption, and limited throughput (Hsu et al., 2003) tend to hinder its development. Ling et al. (2015) evaluated seven drying techniques to assess their impact on *Kappaphycus alvarezii* phytochemical composition and antioxidant activity; the highest levels of phytochemical compounds and improved abilities for free radical scavenging and reducing were obtained through oven-drying at 40 °C. Meanwhile, Chilean green seaweed (*Ulva* spp.) convective drying at 70 °C for 120 min is considered the most effective method for retaining physicochemical parameters and antioxidant capacity, when compared to other drying techniques including freeze-drying, vacuum-drying, and solar-drying (Uribe et al., 2019). Chenlo et al. (2018) investigated and compared the dehydration and rehydration characteristics of *Ascophylum nodosum* and *Undaria pinnatifida*, two brown seaweed types, over a wide range of temperatures relevant in industrial settings. The study concluded that conventional air-drying methods are suitable for *A. nodosum*; however, alternative drying techniques should be investigated to improve *U. pinnatifida* rehydration properties.

Notably, insufficient information is available concerning *B. fusco-purpurea* drying properties. Moreover, there have been limited investigations conducted regarding HAD and VFD impacts on *B. fusco-purpurea* VOC. Hence, comprehensive study of the various drying techniques is warranted.

Developing a rapid, convenient, and energy-efficient drying method is key to realizing the *B. fusco-purpurea* economic value. Accordingly, here, we examined HAD and VFD effects on *B. fusco-purpurea* drying characteristics, microstructure, rehydration, and volatile compounds, subsequently selecting the most appropriate dehydration parameters. The primary aim of this study was to determine how to preserve *B. fusco-purpurea* physical characteristics and flavor quality while providing practical drying information that can be scaled up for industrial use. Based on economic efficiency and product quality principles, our evaluations suggest that HAD remains a viable option for *B. fusco-purpurea* dehydration.

2. Material and methods

2.1. Materials

Fresh *B. fusco-purpurea* was collected from the coastal area of Putian, China, and provided by Putian Hai Dao Ren Jia Aquatic Products Co., Ltd. The samples were transported to the laboratory in seawater at 4 °C and cleaned to remove impurities.

2.2. Drying methods for B. fusco-purpurea

2.2.1. HAD

Fresh *B. fusco-purpurea* weighing 100 ± 0.5 g with a 5-mm thickness were spread on gauze and placed in a hot-air drying oven (BGZ-240, Shanghai Bosen Industrial Co., Ltd. Medical Equipment Factory, China). The drying temperature was 70 °C, and the wind speed was 2 m/s. The *B. fusco-purpurea* initial weight was measured, and the sample was weighed every 0.5 h thereafter until the final product reached a constant weight.

2.2.2. VFD

Fresh *B. fusco-purpurea* weighing 100 ± 0.5 g with a 5-mm thickness were spread on gauze and pre-frozen at -80 °C for 1 h. Subsequently, the samples were placed in the drying chamber (Alpha2-4 LD Plus, Christ, Germany) when the cold trap temperature reached -60 °C. The primary drying was performed at -30 °C and a 0.37 mbar vacuum pressure; the sample weight was measured every hour until the final product achieved a constant weight.

2.3. Determination of dry basis moisture content

The dry-basis moisture content during drying was determined using

Equation (1):

$$M_t = \frac{m_t - m_d}{m_d} \quad (1)$$

where *Mt* represents the *B. fusco-purpurea* dry basis moisture content at time t (g water/g dry basis), m_t is the *B. fusco-purpurea* weight at time t (g), and m_d is the *B. fusco-purpurea* weight after drying to a constant weight, which is the dry basis weight (g).

2.4. Determination of moisture ratio

The moisture ratio (*MR*) represents the amount of water in a material that has not been removed under certain drying conditions and can be used to indicate the drying rate. During the drying process, *MR* was calculated using Equation (2):

$$MR = \frac{Mt}{M_o} \quad (2)$$

where *Mt* is the moisture content on a dry basis at time t (g water/g dry basis), and *Mo* is the initial moisture content on a dry basis (g water/g dry basis).

2.5. Determination of effective diffusivity coefficient

The effective diffusivity coefficient (*Deff*) is a measure of moisture removal ability through diffusion. This can be calculated using Fick's second law (Equation (3)):

$$MR = \frac{8}{\pi^2} exp\left(-\frac{\pi^2 D_{eff}}{L^2} t\right) \quad (3)$$

Taking the logarithm of both sides of Equation (3), we obtain Equation (4):

$$\ln MR = \ln\left(\frac{8}{\pi^2}\right) - \frac{\pi^2 D_{eff}}{L^2} t \quad (4)$$

where *MR* is the moisture ratio, t is the drying time (h), L is the sample thickness (m), and *Deff* is the effective diffusivity coefficient (m^2/h). Plotting ln*MR* on the y-axis and the drying time t on the x-axis yields a linear equation, the slope of which can be substituted into Equation (5) to determine *Deff* for moisture (Vega-Gálvez et al., 2010):

$$D_{eff} = -\frac{L^2}{\pi^2} k \quad (5)$$

2.6. Observation with scanning electron microscopy (SEM)

A dry sample of *B. fusco-purpurea* was fixed onto a conductive sample holder using conductive adhesive tape. The sample was then subjected to vacuum and coated with a layer of gold via sputtering to ensure conductivity. The sample holder was then positioned in a low-temperature scanning electron microscope (SU8100, Hitachi, Ltd., Japan), and its microstructure was observed under an acceleration voltage of 5 kV.

2.7. Determination of rehydration ratio

The rehydration ability of the sample was represented by the rehydration ratio (*RR*), determined by soaking the dried *B. fusco-purpurea* samples in distilled water at 25 °C for rehydration testing. The sample was removed every minute, and the surface was wiped dry with absorbent paper, weighed, and placed back into the water for rehydration. This process was repeated until the weight of the sample stabilized and remained constant. *RR* was calculated as follows (Equation (6)):

$$RR = \frac{W_t - W_O}{W_O} \quad (6)$$

where, W_0 represents the weight of the sample before rehydration and *Wt* is the weight of the sample at time t during rehydration.

2.8. Observation with inverted fluorescence microscopy

To visualize the effects of different drying techniques on the rehydration performance of *B. fusco-purpurea*, an inverted fluorescence microscope (ECLIPSE Ts2R-FL, Nikon Corporation, Japan) was used to observe the microstructure of fresh and rehydrated samples. Fresh and dried *B. fusco-purpurea* were placed in water, and intact single-layer *B. fusco-purpurea* was selected and placed on a glass slide. Characteristic microstructure images of the samples were captured and photographed at 10 × 40 magnification.

2.9. Electronic nose (e-nose) analysis

The e-nose sensor array (PEN3.5, AIRSENSE Analytics GmbH, Germany) comprises ten metal oxide sensors (named beginning with "W"), each with specific functions: W1C responds well to aromatic compounds, W5S is sensitive to nitrogen oxides, W3C shows sensitivity to ammonia and aromatic compounds, W6S can selectively detect hydrides, W5C responds to short-chain alkane aromatic compounds, W1S detects methyl compounds, W1W is responsive to sulfides, W2S detects alcohols and aldehydes/ketones, W2W has an affinity for aromatic compounds and organic sulfides, and W3S is sensitive to long-chain alkanes (Wu et al., 2021).

To conduct the experiment, 0.8 g of *B. fusco-purpurea* dried by HAD, 0.8 g of *B. fusco-purpurea* dried by VFD, and 2.5 g of fresh *B. fusco-purpurea* were placed in e-nose collection bottles, sealed, and left at room temperature (25 °C) for 60 min until the sample in the tube reached equilibrium with the gas phase. The e-nose detected volatile odors, with three replicates per group. The measurement conditions were as follows: sensor cleaning time of 200 s, zeroing time of 10 s, sample preparation time of 5 s, sample testing time of 200 s, and internal flow rate of 200 mL/min. Data from 150 to 152 s were selected for subsequent analyses based on preliminary experiments to ensure the data's stability and accuracy. Principal component analysis (PCA) was used to cluster and discriminate the different samples.

2.10. Headspace (HS-) solid-phase microextraction (SPME) combined with comprehensive two-dimensional gas chromatography time-of-flight mass spectrometry (GC × GC-TOF MS) detection

2.10.1. Conditions of HS-SPME

The experimental conditions for HS-SPME were determined by slightly modifying the parameters set by Liu et al. (2021). The HAD *B. fusco-purpurea* (0.8 g), VFD *B. fusco-purpurea* (0.8 g), and fresh *B. fusco-purpurea* (2.5 g) were separately weighed and placed in a 20-mL headspace vial. Three replicates were collected from each group. Subsequently, the vial was incubated at 50 °C for 15 min, and SPME was performed at 50 °C for 30 min. Subsequently, desorption of divinylbenzene/carboxen/polydimethylsiloxane fibers was carried out in a splitless injection gas chromatography (GC) mode at 250 °C for 180 s.

2.10.2. Conditions of GC × GC-TOF MS

The GC × GC-TOF MS system utilized here was an Agilent Technologies 7890 B GC system, which was paired with an SSM1810 solid-state thermal modulator, HV modulation column (Snow Scene Electronic Technology (Shanghai) Co., Ltd.), and HeXin (EI-0610, HeXin Analytical Instrument, China) time-of-flight mass spectrometer.

GC conditions: The GC columns comprised a DB-WAX (30 m × 0.25 mm × 0.25 μm) as the first dimension column and a DB-17MS (1.0 m × 0.15 mm × 0.15 μm) as the second dimension column. Helium (purity ≥99.999%) was the carrier gas. The injection mode was splitless, and the column flow rate was 1.0 mL/min. The column temperature program

was as follows: initial temperature of 40 °C, held for 5 min, and then increased at 4 °C/min to 240 °C.

Mass spectrometry (MS) conditions: The transfer line temperature was 240 °C, and the electron ionization temperature was 220 °C. The detector voltage was -1850 V, and the electron ionization energy was 70 eV. The samples were subjected to SPME. A signal of 40–400 amu was acquired at 100 Hz.

Qualitative analysis of the VOC was performed using Canvas 2.5, a comprehensive two-dimensional (2D) chromatography data processing software, combined with the NIST 20 mass spectrum library. The samples were classified, aligned, and compared using the software of Album 1.0 comprehensive 2D chromatography multi-sample comparison analysis. Feature difference analysis was performed using the Fisher Ratio algorithm (with peak area weighting, group distance minus group fluctuation), and the top 50 compounds were compared.

2.11. Data processing and analysis

The plotting task was accomplished using OriginPro2018 software (OriginLab Corp., Northampton, MA, USA) in conjunction with Evolutionary Genotype-Phenotype Systems software (Yu et al., 2019).

3. Results and discussion

3.1. Effect of different drying methods on B. fusco-purpurea drying kinetics

The moisture ratio change curves of *B. fusco-purpurea* during the VFD and HAD processes were illustrated in Fig. 1A. As the drying time increased, the moisture ratio of *B. fusco-purpurea* exhibited an exponential decrease. The moisture ratio decreased rapidly in the initial phases, whereas it gradually decreased in the later stages, owing to the increased energy required to extract bound water (Ren et al., 2021). Additionally, various drying techniques significantly impacted changes in the moisture ratio of *B. fusco-purpurea*. The required time for VFD *B. fusco-purpurea* was 3.7 times higher than that of HAD, while Xu et al. (2020) VFD required 24 h to reach the same final water content as hot air drying, which took only 8.5 h to dry cabbage. Furthermore, the time required for ginger VFD was 3.7 times greater than hot air drying (An et al., 2016). Aware and Thorat (2011) compared the drying kinetics of garlic using different drying methods and found that freeze-drying required 3–5 times more time than hot drying. The VFD freezes the material to a eutectic point or lower. After the water becomes solid, the material enters the main drying stage. Under vacuum conditions, the frozen water in the material changes from solid to gas through sublimation, removing moisture from the material (Ratti, 2001). During the VFD process, heat was transferred to *B. fusco-purpurea* solely through the difference in temperature between the zones of freezing and drying. The flow of heat was oriented from the exterior toward the interior, whereas the driving force of mass transfer, which occurred from the inside to the outside, was the difference in vapor pressure between *B. fusco-purpurea* and cold butane. However, as time was also required to establish a sufficient vapor pressure difference, the drying time of VFD was noticeably longer than that of HAD. In contrast, HAD derived its heat source from the drying equipment, meaning that the fan blew heat to all parts of the equipment. The heat circulated around *B. fusco-purpurea* and gradually diffused from the surface toward the cell's interior until the moisture evaporated. Ong and Law (2011) found that heat treatment increased the intercellular space, ruptured the cell membrane, and reduced the tissue angle of cell adhesion, all of which contribute to reducing the flow resistance of water and improving the drying rate. Therefore, the hot-air drying time was shorter.

The drying process involves the transfer of momentum, mass, and energy. When low-temperature materials absorb heat from the drying medium, heat is transferred from the exterior to the interior of the particles, whereas the moisture within the particles is transferred to the exterior. After reaching the critical moisture level, the drying process ends, and the heat inside the particles is transferred via thermal conduction, whereas moisture is transferred via diffusion (Komatsu et al., 2015). The liquid diffusion theory was used in the food material drying process without considering the driving force of diffusion to simplify the calculation results. All of the dynamic effects were incorporated into the diffusion coefficient using the effective moisture diffusion coefficient (D_{eff}) to characterize the average speed of moisture migration during the drying process (Zheng et al., 2014). D_{eff} was calculated using the slope method, where ln(*MR*) was linearly fitted to the drying time (t) (Fig. 1B), with R^2 values > 0.90, indicating good fitting results. The D_{eff} for VFD was 3.7386×10^{-10} m^2/s, whereas that for HAD was 1.5674×10^{-9} m^2/s, both falling within the Deff range of D_{eff} 10^{-10} m^2/s to 10^{-8} m^2/s for food materials (Liu et al., 2014). The findings suggest that HAD demonstrated greater effectiveness in removing moisture compared to VFD.

3.2. Effects of different drying techniques on the microstructure of B. fusco-purpurea

The different drying methods affected the microstructure of *B. fusco-purpurea* (Fig. 2). In contrast to the wrinkled surfaces of the HAD samples (Fig. 2A_1), the surfaces of the samples obtained by VFD were relatively flat and smooth (Fig. 2B_1), similar to the results of Huang et al. (2011). Moreover, after drying by HAD, the *B. fusco-purpurea* appeared as a solid column-shaped bar, therefore increasing the hardness of the sample (Fig. 2A_2), whereas the skeletal structure of *B. fusco-purpurea* dried using VFD remained relatively intact (Fig. 2B_2) which may be due to the removal of moisture through sublimation under vacuum conditions (Zhang et al., 2020). Meanwhile, any drying process involving heat causes the sample to exhibit uneven moisture and temperature

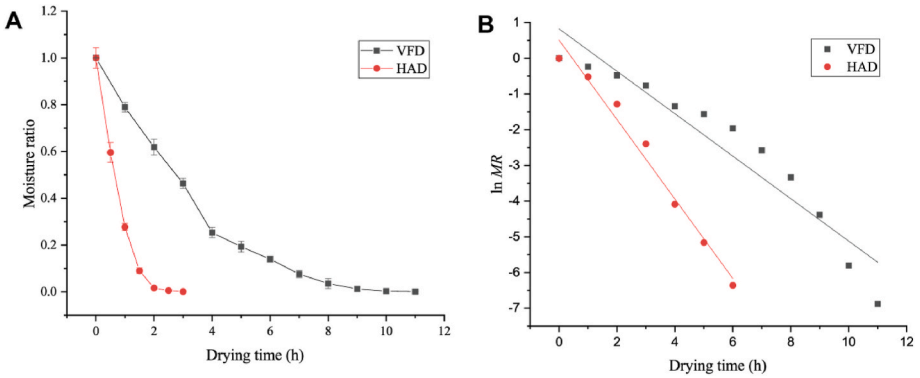

Fig. 1. Effects of different drying techniques on the drying characteristics of *Bangia fusco-purpurea.* (A) Moisture ratio changes over times of *Bangia fusco-purpurea* dried by vacuum freeze-drying (VFD) and hot air drying (HAD); (B) Relationship curves between ln*MR* (natural logarithm of moisture ratio) and drying time.

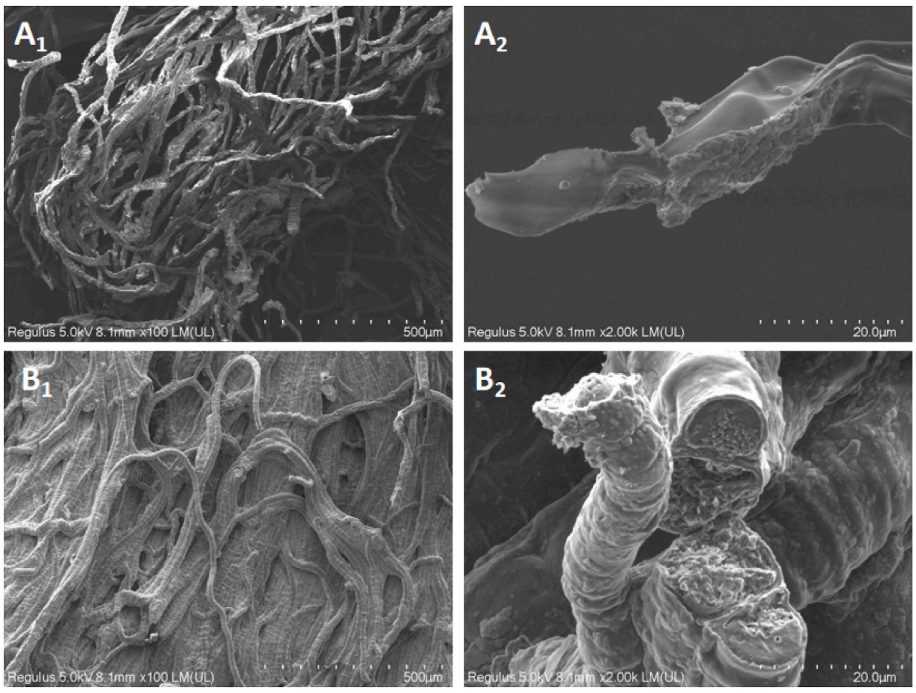

Fig. 2. Effects of different drying techniques on the microstructure of *B. fusco-purpurea.* (A) hot air drying (HAD) *B. fusco-purpurea*; (B) vacuum freeze-drying (VFD) *B. fusco-purpurea*. The subscript numerics 1 and 2 denote a magnification of 100 times and 2000 times, respectively.

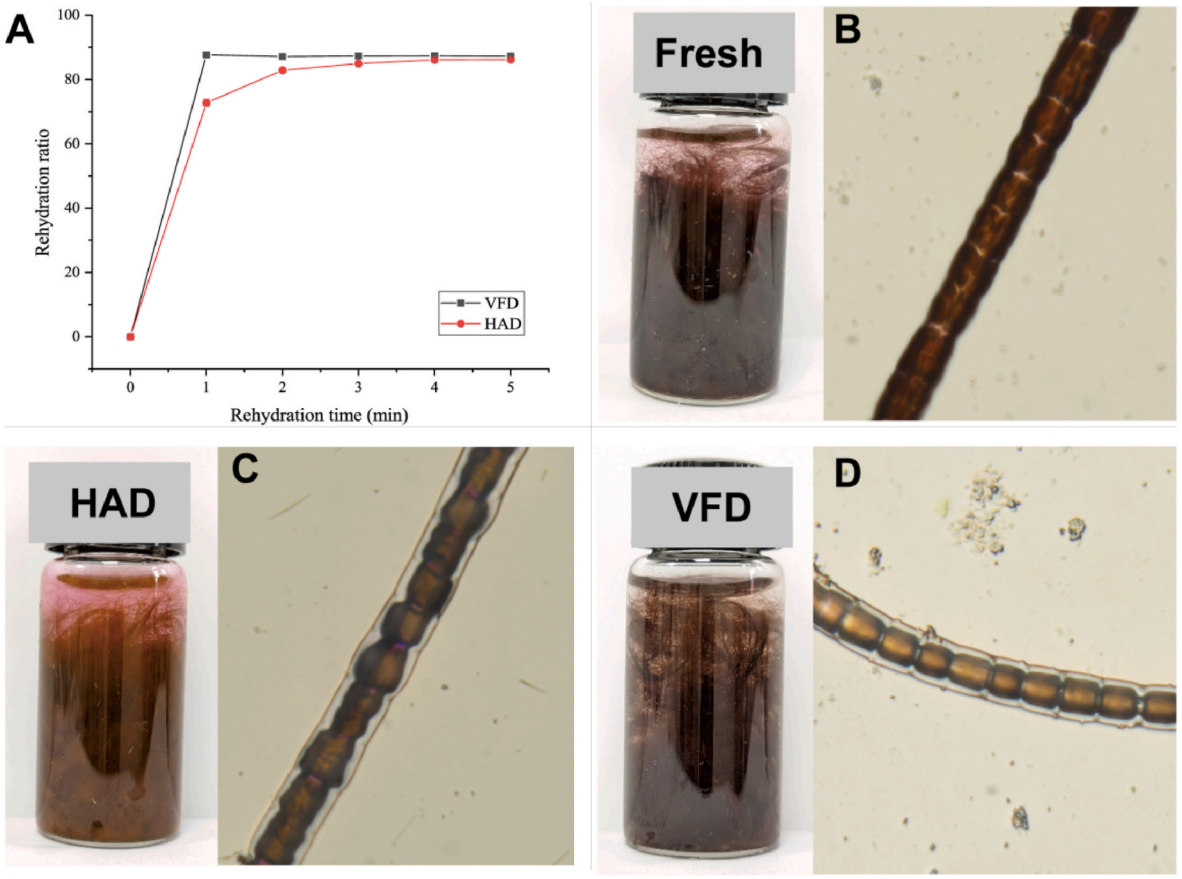

Fig. 3. Rehydration characteristics of dried *B. fusco-purpurea*. (A) The rehydration ratio changes over times for *B. fusco-purpurea* with different drying techniques; (B) Optical microscopy images of fresh *B. fusco-purpurea* magnified by 10 × 40 times; (C) Optical microscopy images of HAD *B. fusco-purpurea* magnified by 10 × 40 times; (D) Optical microscopy images of VFD *B. fusco-purpurea* magnified by 10 × 40 times. Photograph of the bottles: States of *B. fusco-purpurea* after rehydration.

gradients, resulting in degradation, deformation, and folding (Chumroenphat et al., 2021). A correlation exists between the microstructure and surface shrinkage of dried products with the water migration mechanism and external pressure variations (An et al., 2016). During HAD, *B. fusco-purpurea* was exposed to high temperatures of 70 °C for a remarkable amount of time, resulting in significant damage to the seaweed's skeleton structure, dehydration caused the collapsion of the seaweed cells, leading to severe shrinkage and hardening of the *B. fusco-purpurea*'s surface. Moreover, the loss of moisture and heating may cause an increase in pressure on the cell structure of foods, reducing cell framework rigidity and resulting in shrinkage, collapse, and changes in the microstructure of *B. fusco-purpurea* cells.

3.3. Effect of different drying methods on the water rehydration properties of dried B. fusco-purpurea

Drying can cause irreversible damage to the tissue structures of samples. Thus, the water rehydration ratio is an essential indicator of the degree of damage to the internal tissue structure during the drying process. The different drying methods were found to have different effects on the water-rehydration properties of *B. fusco-purpurea* (Fig. 3). After 1 min of rehydration, the water rehydration ratio of *B. fusco-purpurea* dried by VFD was 87.64%, which remained stable. In contrast, the water rehydration ratio of *B. fusco-purpure* dried by HAD was only 72.77%, and 4 min were required to reach stability at a water rehydration ratio of 86.12%. The HAD samples turned brown to purplish-red (Fig. 3C), whereas VFD samples remained closer to fresh *B. fusco-purpurea* (Fig. 3D). This may be due to the HAD samples being subjected to a high temperature (70 °C) for a long time, thereby damaging the internal tissue structure and causing the collapse of micro-pore channels, leading to the loss of contents. Furthermore, the intensification of shrinkage and surface hardening may hinder water penetration during rehydration (Rojas and Augusto, 2018). In contrast, the temperature during VFD was lower, resulting in less damage to the cells and preservation of the original color to the greatest extent possible (Zhang et al., 2020). The VFD samples presented a porous network structure filled with air, as the rehydration process comprised the exchange of gas from inside the sample space with moisture from the outside (Feng et al., 2020). Thus, the water rehydration rate of the VFD samples was higher than that of the HAD samples.

The microscopic structure of the post-rehydration samples was observed using an optical microscope, and images of the characteristic microscopic structures of the samples were captured at 10 × 40 magnification to visualize the impact of different drying techniques on the rehydration ratio of *B. fusco-purpurea*. The cell tissue of fresh *B. fusco-purpurea* was relatively dense (Fig. 3B), whereas the dried and rehydrated cells became separated (Fig. 3C and Fig. 3D). Drying treatment will cause varying degrees of damage to the cells, and during the rehydration process, the *B. fusco-purpurea* continuously absorbs water, causing internal pressure to increase and some cell structures to deform, leading to increased spacing between the cells. Different drying treatments resulted in varying degrees of cell damage, with the VFD technique better preserving the original appearance of *B. fusco-purpurea* (Zhang et al., 2020), while the HAD technique induced apparent damage and deformation. Therefore, the cell structure of the VFD sample was more uniform than that of the HAD sample after rehydration.

3.4. Determination of VOC by e-nose

Electronic nose analysis showed that each odor produced a specific group of organic and inorganic gases. The response values of the ten sensors in the e-nose detection system for fresh, HAD, and VFD *B. fusco-purpurea* odors were depicted in Fig. 4A. The analysis revealed that the response values from the W1C, W3C, W6S, W5C, and W3S sensors to fresh and dried *B. fusco-purpurea* odors did not differ significantly. However, prominent differences in response values were observed for the W5S, W1S, W1W, W2S, and W2W sensors. The response values of the W1S and W2S sensors differed significantly between HAD and VFD *B. fusco-purpurea*, whereas those of the other sensors were similar. HAD and VFD remarkably reduced the levels of sulfides, aromatic components, and nitrogen oxides in fresh *B. fusco-purpurea* odors. Moreover, the levels of alcohol and aldehyde compounds in HAD samples were significantly lower than those in other samples, whereas the levels of methyl compounds in VFD samples were significantly higher than those in other samples. Cluster discrimination analysis was conducted on various samples utilizing PCA (Fig. 4B). Notably, the first (PC1) and second principal components (PC2) had variance contribution rates of 53.80 % and 44.40 %, respectively, amounting to a cumulative variance contribution rate of 98.20 %, indicating that these two factors held most of the sample information. The PCA revealed significant differences in odor among the three samples.

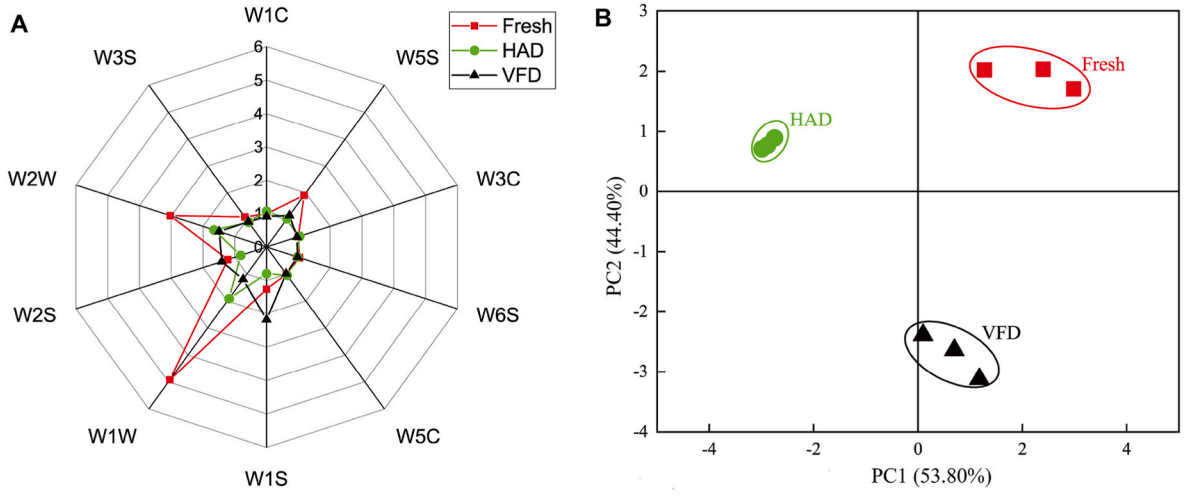

Fig. 4. Analysis of volatile profiles by electronic nose (e-nose). (A) Radar plot of e-nose data from fresh and drying *B. fusco-purpurea*. Regarding the type of response of electronic nose sensors to substances, W1C responds to aromatic compounds, W5S responds to nitrogen oxides, W3C responds to ammonia and aromatic compounds, W6S responds to hydrides, W5C responds to short-chain alkane aromatic compounds, W1S responds to methyl compounds, W1W responds to sulfides, W2S responds to alcohols and aldehydes/ketones, W2W responds to aromatic compounds and organic sulfides, and W3S responds to long-chain alkanes. (B) Principal component analysis (PCA) of e-nose output data.

3.5. Determination of VOC by HS-SPME coupled with GC × GC-TOF MS

Fig. 5 displays the 2D chromatographic profile and three-dimensional (3D) view of the GC × GC-TOF MS of the VOC of *B. fusco-purpurea* manufactured using different drying techniques. The horizontal axis of the 2D spectra represents the first-dimension retention time, whereas the vertical axis represents the second-dimension retention time. The signal intensity of the total ion chromatogram is illustrated in color, with blue to red indicating signal intensities from weak to strong. The detection method uses a reverse column configuration with a polar column in the first dimension and a moderately polar column in the second. Hence, the more polar the component in the sample, the shorter its retention time on the second dimension column. In the graph, the component peaks are arranged from top to bottom according to their polarity, with the compound families in the order of alkanes, alkenes, aldehydes/ketones, heterocyclics, alcohols/esters, and acids, based on their similar 2D retention times.

The VOC in *B. fusco-purpurea* were identified using the Canvas2.5 comprehensive 2D chromatographic data processing software, which utilized the NIST 20 mass spectrum library. Nine compounds were identified: esters, alcohols, ketones, hydrocarbons (aromatic hydrocarbons, alkanes, alkenes, dienes, cyclic alkenes, substituted hydrocarbons, cyclic hydrocarbons, and alkynes), aldehydes, ethers, phenols, acids, and heterocyclic compounds. The results (Fig. 6) show that an average of 399 compounds were detected in fresh *B. fusco-purpurea* samples, 449 compounds in VFD samples, and 352 compounds in HAD samples, indicating a reduction in the total number of volatile compounds, possibly due to the degradation of flavor precursors caused by exposure to high temperatures (Zhang et al., 2019).

During high-temperature drying, alcohols undergo esterification reactions (Carrapiso et al., 2002), resulting in a significant decrease in alcohol compounds after being subjected to 70 °C HAD, while *B. fusco-purpurea* treated with VFD remained relatively unchanged. Ester compounds primarily use amino acids, sugars, and lipids as biosynthetic precursors, resulting in the emergence of new ester compounds during the drying process, primarily through lipid oxidation and esterification reactions of free fatty acids and alcohols (Chen et al., 2017). Although HAD and VFD have been found to reduce the quantity and diversity of ester compounds in *Ganoderma lucidum*, few studies have indicated that heating promotes the formation of ester compounds, including the abundant production of 1-propen-2-ol acetate after HAD (Liu et al., 2021). Moreover, *B. fusco-purpurea* exhibited a significant increase in the variety of ester compounds after VFD whereas the variety increased only slightly after HAD.

It is hypothesized that aldehydes originate from the auto-oxidation or enzymatic degradation of polyunsaturated fatty acids (PUFAs). Aldehydes in the range of C6–C9 exhibit a fatty-green aroma, while those in the range of C15–C17 have a distinct marine seaweed scent (Francezon et al., 2021). In addition to aldehydes, PUFAs can be converted into ketones via degradation (Francezon et al., 2021). After drying, the types of ketone compounds were reduced, and the VFD samples displayed notably elevated concentrations compared to other samples. Sulfur compounds exhibit distinctive algal scents due to their strong odoriferous properties, although these compounds may exist in small amounts and possess extremely low odor thresholds (Sánchez-García et al., 2021; Yao et al., 2022). When subjected to HAD or VFD, there were minimal alterations in the variations and amounts of aldehyde- and sulfur-containing compounds. This suggests that the typical flavor associated with algae remained intact following the drying procedure. Hydrocarbon compounds generally tend to possess a high threshold and exhibit a strong pungent odor, which typically makes the sample less flavorful (Zhang et al., 2019). The number of hydrocarbon compound types was higher in the VFD samples than in the HAD samples. Therefore, VFD samples possessed a stronger aroma when compared with HAD samples, which is consistent with the sensory evaluation result.

According to the compound peak list, the samples were classified,

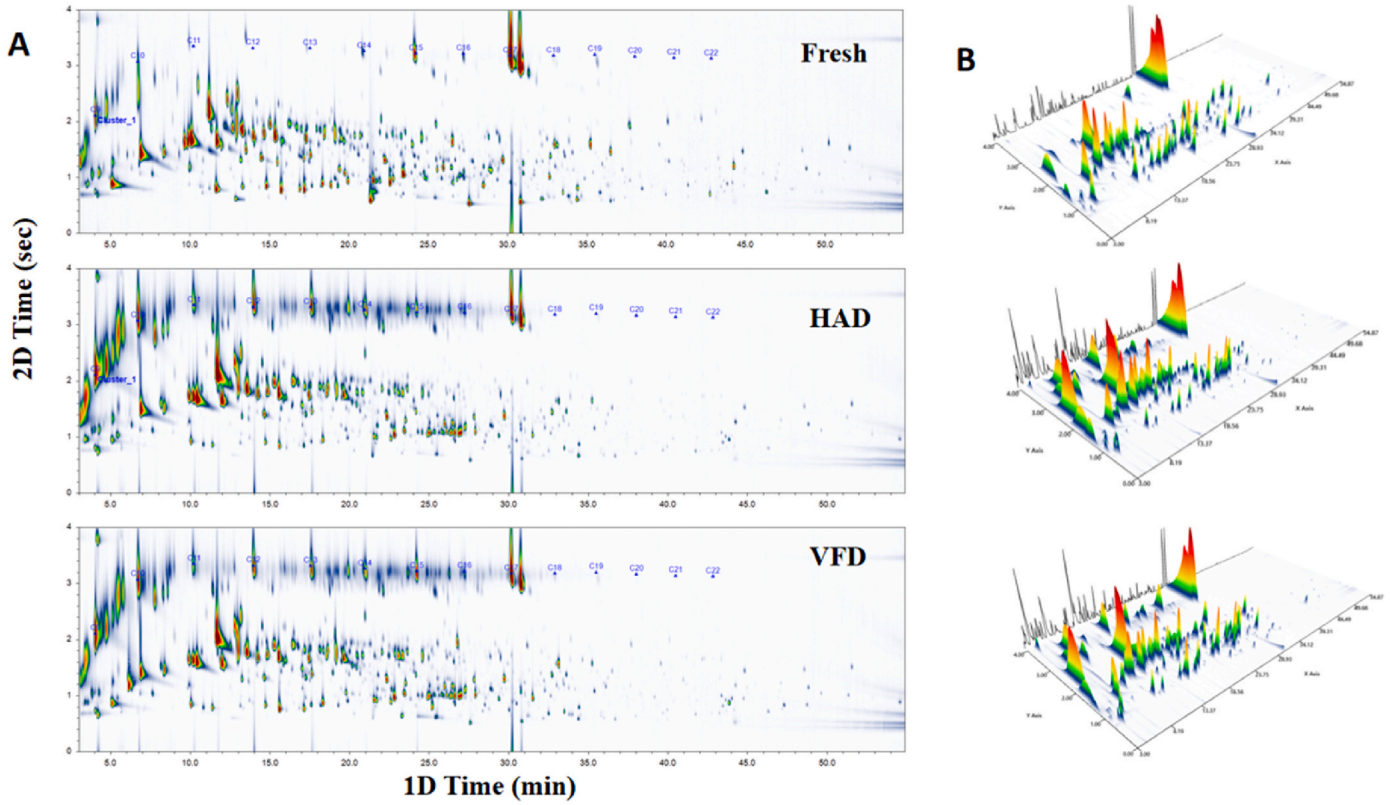

Fig. 5. GC × GC-TOF MS (two-dimensional [2D] gas chromatography-time-of-flight mass spectrometry) spectra of *B. fusco-purpurea* VOC obtained by different drying methods. (A) Comprehensive 2D chromatography-flight mass spectra. (B) Three-dimensional topographical visualization.

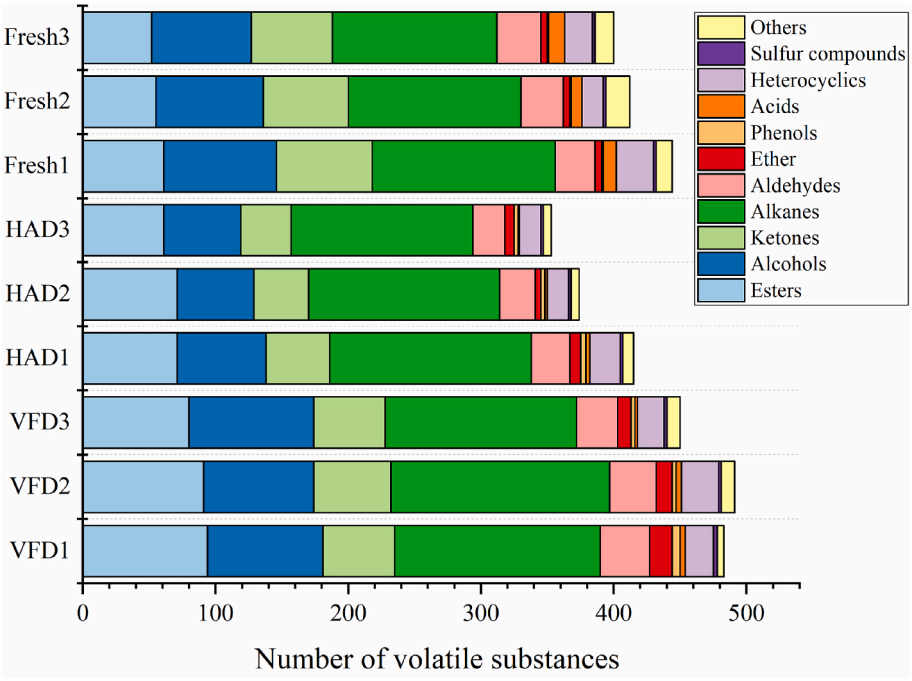

Fig. 6. Chemical species in fresh, HAD, and VFD *B. fusco-purpurea.*

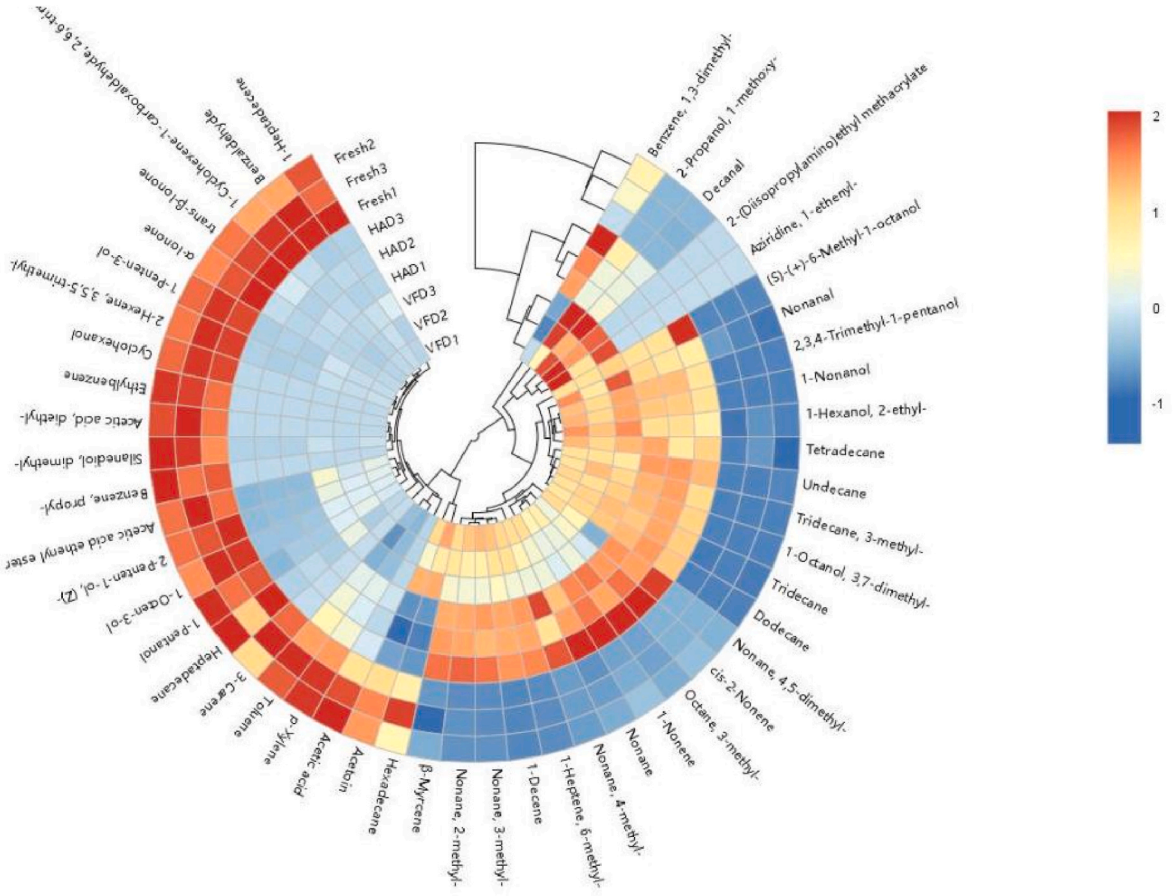

Fig. 7. Thermal image analysis and hierarchical clustering dendrogram of *B. fusco-purpurea* volatile compounds obtained by different drying techniques. The numbers correspond to the identified signals.

aligned, and compared using Album 1.0 comprehensive 2D chromatographic data processing software. The top 50 volatile compounds with the most significant differences were selected for heatmap and cluster analyses (Fig. 7). The relative content of each volatile substance after different drying treatments is marked with different colors in the heatmap, with red and blue indicating high- and low-content areas, respectively. The deeper the red or blue color, the higher or lower the relative content, respectively. Cluster analysis revealed good parallelism within each set of samples, with minor differences between HAD and VFD samples but significant differences between fresh samples.

As observed in Fig. 7, the content of VOC, namely 1-heptadecene, benzaldehyde, 2,6,6-trimethyl-1-cyclohexene-1-carboxaldehyde, trans-β-Ionone, α-Ionone, 1-penten-3-ol, (Z)-2-penten-1-ol, 3,5,5-trimethyl-2-hexene, cyclohexanol, ethylbenzene, diethyl-acetic acid, dimethyl-silanediol, propyl-benzene, acetic acid ethenyl ester, (Z)-2-penten-1-ol, 1-octen-3-ol, 1-pentanol, heptadecane, 3-carene, toluene, p-xylene, and acetic acid, were decreased after HAD and VFD.

New VOC (dodecane, 1-decene, 4,5-dimethyl-nonane, 3-methyl-nonane, 4-methyl-nonane, 1-nonanol, 3-methyl-tridecane, (S)-(+)-6-methyl-1-octanol) were produced in the *B. fusco-purpurea* samples subjected to HAD and VFD. Only VFD samples contained 2-(diisopropylamino)ethyl methacrylate and 1-ethenyl-aziridine. Moreover, during HAD, a significant decrease was observed in the acetoin and hexadecane content. However, the levels in VFD and fresh *B. fusco-purpurea* remained relatively constant.

Using PCA for cluster discriminant analysis of different samples, Fig. 8 shows the score and loading plots of the samples. The PC1 and PC2 contributed to the variance rates by 82.20% and 13.70%, respectively, with a cumulative variance contribution rate of 95.90% (Fig. 8A). The three samples were divided in the score plot, similar to the results for the e-nose. Regarding PC1, there were significant differences among the HAD, VFD, and fresh samples. Regarding PC2, there were significant differences between the HAD and VFD groups, and the fresh sample was located between them. In the loading plot (Fig. 8B), each component was divided into four groups according to the quadrant, with attributes in the same group having a close positive correlation. Approximately all variables were within the 95% confidence interval, meaning the model can explain these variables well.

4. Conclusions

Here, the drying characteristics and volatile profiles of *B. fusco-purpurea* were investigated in detail using HAD and VFD. It was revealed that the drying efficiency of HAD was superior to that of VFD, evidenced by the notable differences in drying time, with VFD taking 3.7 times longer than HAD. Adversely the continuous high temperature of 70 °C during HAD led to the shrinkage, collapse, and deformation of the microstructure of *B. fusco-purpurea*. After a rehydration period of 4 min, the sample achieved stability, with a rehydration ratio of 86.12%. Significant differences between HAD samples and fresh *B. fusco-purpurea* were observed in cell structure damage after rehydration. The surface of the VFD sample was relatively complete and smooth, and after a brief rehydration period of 1 min, the sample achieved stability with a rehydration ratio of 87.64%; the sample was closer to fresh *B. fusco-purpurea* after rehydration, indicating that VFD can better preserve the physical and chemical characteristics of *B. fusco-purpurea*.

E-nose results indicated that the response values of the HAD and VFD *B. fusco-purpurea* were notably distinct for the W1S and W2S sensors, which were sensitive to methyl, alcohol, aldehyde, and ketone, respectively. The response values of the other sensors were relatively similar. Both drying methods significantly reduced the sulfide, aromatic components, and nitrogen oxide compounds in fresh *B. fusco-purpurea*; conversely, the content of methyl flavor substances in VFD samples was significantly higher than in the others, and the HAD, VFD, and fresh red hair algae samples were well distinguished via PCA.

GC × GC-TOF MS analysis of fresh, HAD, and VFD *B. fusco-purpurea* revealed the presence of 399, 352, and 449 volatile compounds, respectively. Nine volatile categories were identified in the three types of *B. fusco-purpurea*, with hydrocarbons, alcohols, and esters being the most abundant chemical classes. Thermogram and cluster analyses demonstrated that the drying process significantly affected the volatile components of *B. fusco-purpurea*. Substances including benzaldehyde, 2,6,6-trimethyl-1-cyclohexene-1-formaldehyde, and α-ionone were significantly reduced in both HAD and VFD samples. As drying progressed, hydrocarbons and alcohols were generated in the HAD and VFD samples owing to the thermal degradation of carbohydrates, lipids, amino acids, and Maillard reactions. The content of acetoin and hexadecane in HAD samples was significantly lower, while that of 1,3-dimethylbenzene was significantly higher. The contents of 1-methoxy-2-propanol, decanal, 1-ethenyl-aziridine and 2-(diisopropylamino)ethyl methacrylate in VFD samples were significantly higher.

HAD has a better drying efficiency than VFD. However, VFD can greatly preserve the quality of products. Different drying methods for *B. fusco-purpurea* resulted in significant differences in the types and amounts of volatile aroma constituents. The initial exploration into the impact of the drying procedure on the quality and flavor of *B. fusco-purpurea* has provided preliminary theoretical and technical support for the further development of high-quality dried *B. fusco-purpurea*. Based on this, future research should be conducted to shorten the drying time of VFD, improve the drying efficiency, and elucidate the formation mechanism of key flavor substances during the drying process.

CRediT authorship contribution statement

Jingna Wu: Conceptualization, Methodology, Investigation, Writing, Visualization. **Nan Pan:** Methodology, Writing, Formal analysis, Visualization. **Xiaoting Chen:** Writing, Formal analysis. **Debiao Shan:** Formal analysis. **Huifang Shi:** Formal analysis. **Yingshan Qiu:**

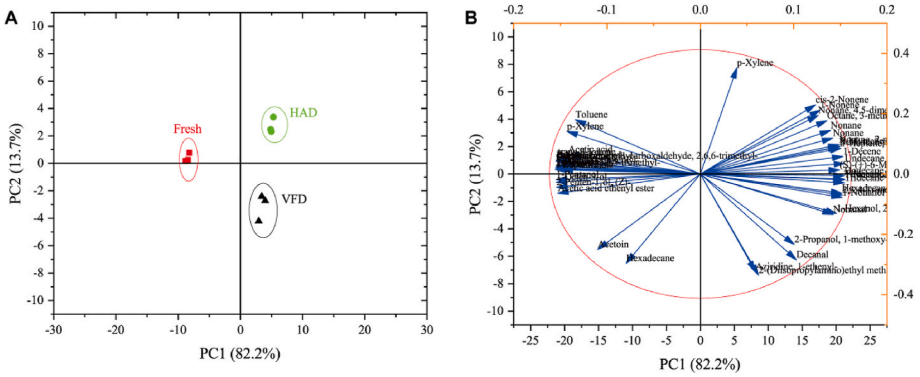

Fig. 8. PCA of the volatile components of fresh, HAD, and VFD *B. fusco-purpurea*. (A) PCA score plot; (B) PCA loading plot.

Formal analysis. **Zhiyu Liu:** Funding acquisition. **Yongchang Su:** Resources. **Junfa Weng:** Resources.

Declaration of competing interest

The authors declare that they have no known competing financial interests or personal relationships that could have appeared to influence the work reported in this paper.

Data availability

Data will be made available on request.

Acknowledgements

This work was supported by the Youth Science and Technology Innovation Program of Xiamen Ocean and Fisheries Development Special Funds [grant number 23YYST079QCA12] and Fujian Provincial Science and Technology Plan [grant number 2022N3004].

References

An, K., Zhao, D., Wang, Z., Wu, J., Xu, Y., Xiao, G., 2016. Comparison of different drying methods on Chinese ginger (*Zingiber officinale* Roscoe): changes in volatiles, chemical profile, antioxidant properties, and microstructure. Food Chem. 197 (B), 1292–1300. https://doi.org/10.1016/j.foodchem.2015.11.033.

Aware, R.S., Thorat, B.N., 2011. Garlic under various drying study and its impact on allicin retention. Dry. Technol. 29 (13), 1510–1518. https://doi.org/10.1080/07373937.2011.578230.

Carrapiso, A.I., Jurado, A., Timón, M.L., García, C., 2002. Odor-active compounds of Iberian hams with different aroma characteristics. J. Agric. Food Chem. 50 (22), 6453–6458. https://doi.org/10.1021/jf025526c.

Chen, G.T., Wu, F.N., Pei, F., Cheng, S., Muinde, B., Hu, Q., Zhao, L., 2017. Volatile components of white Hypsizygus marmoreus detected by electronic nose and HS-SPME-GC-MS: influence of four drying methods. Int. J. Food Prop. 20 (12), 2901–2910. https://doi.org/10.1080/10942912.2016.1258575.

Chenlo, F., Arufe, S., Díaz, D., Torres, M.D., Sineiro, J., Moreira, R., 2018. Air-drying and rehydration characteristics of the brown seaweeds, *Ascophylum nodosum* and *Undaria pinnatifida*. J. Appl. Phycol. 30 (2), 1259–1270. https://doi.org/10.1007/s10811-017-1300-6.

Chumroenphat, T., Somboonwatthanakul, I., Saensouk, S., Siriamornpun, S., 2021. Changes in curcuminoids and chemical components of turmeric (*Curcuma longa* L.) under freeze-drying and low-temperature drying methods. Food Chem. 339, 128121 https://doi.org/10.1016/j.foodchem.2020.128121.

Feng, Y.B., Ping Tan, C.P., Zhou, C.S., Yagoub, A.E.A., Xu, B., Sun, Y., Ma, H., Xu, X., Yu, X., 2020. Effect of freeze–thaw cycles pretreatment on the vacuum freeze-drying process and physicochemical properties of the dried garlic slices. Food Chem. 324, 126883 https://doi.org/10.1016/j.foodchem.2020.126883.

Francezon, N., Tremblay, A., Mouget, J.L., Pasetto, P., Beaulieu, L., 2021. Algae as a source of natural flavors in innovative foods. J. Agric. Food Chem. 69 (40), 11753–11772. https://doi.org/10.1021/acs.jafc.1c04409.

Fudholi, A., Sopian, K., Othman, M.Y., Ruslan, M.H., 2014. Energy and exergy analyses of solar drying system of red seaweed. Energy Build. 68, 121–129. https://doi.org/10.1016/j.enbuild.2013.07.072.

Hsu, C.-L., Chen, W., Weng, Y.-M., 2003. Chemical composition, physical properties, and antioxidant activities of yam flours as affected by different drying methods. Food Chem. 83 (1), 85–92. https://doi.org/10.1016/S0308-8146(03)00053-0.

Huang, T.C., Chung, C.C., Wang, H.Y., Law, C., Chen, H., 2011. Formation of 6-shogaol of ginger oil under different drying conditions. Dry. Technol. 29 (16), 1884–1889. https://doi.org/10.1080/07373937.2011.589554.

Jiang, Z., He, P., Wu, L., Yu, G., Zhu, Y., Li, L., Ni, H., Oda, T., Li, Q., 2021. Structural characterization and pro-angiogenic property of a polysaccharide isolated from red seaweed *Bangia fusco-purpurea*. Int. J. Biol. Macromol. 181, 705–717. https://doi.org/10.1016/j.ijbiomac.2021.03.123.

Komatsu, Y., Sciazko, A., Zakrzewski, M., Kimijima, S., Hashimoto, A., Kaneko, S., Szmyd, J.S., 2015. An experimental investigation on the drying kinetics of a single coarse particle of Belchatow lignite in an atmospheric superheated steam condition. Fuel Process. Technol. 131, 356–369. https://doi.org/10.1016/j.fuproc.2014.12.005.

Ling, A.L.M., Yasir, S., Matanjun, P., Abu Bakar, M.F., 2015. Effect of different drying techniques on the phytochemical content and antioxidant activity of *Kappaphycus alvarezii*. J. Appl. Phycol. 27 (4), 1717–1723. https://doi.org/10.1007/s10811-014-0467-3.

Liu, Y.J., Qian, Y.Y., Shu, B., Liu, Y.Y., Tu, X.H., Ouyang, H.J., Li, Y., Tan, G., Yu, Z.W., Chen, F., Lin, L.J., 2021. Effects of four drying methods on *Ganoderma lucidum* volatile organic compounds analyzed via headspace solid-phase microextraction and comprehensive two-dimensional chromatography-time-of-flight mass spectrometry. Microchem. J. 166.

Liu, Y., Liao, Y., Guo, M., Zhang, W., Sang, Y., Wang, H., Cheng, S., Chen, G., 2022. Comparative elucidation of bioactive and volatile components in dry mature jujube fruit (*Ziziphus jujuba* Mill.) subjected to different drying methods. Food Chem. X 14, 100311. https://doi.org/10.1016/j.fochx.2022.100311.

Liu, Y., Wu, J., Miao, S., Chong, C., Sun, Y., 2014. Effect of a modified atmosphere on drying and quality characteristics of carrots. Food Bioprocess Technol. 7 (9), 2549–2559. https://doi.org/10.1007/s11947-014-1295-9.

López-Pérez, O., Del Olmo, A., Picon, A., Nuñez, M., 2020. Volatile compounds and odour characteristics during long-term storage of kombu seaweed (Laminaria ochroleuca) preserved by high pressure processing, freezing and salting. Lebensm. Wiss. Technol. 118, 108710 https://doi.org/10.1016/j.lwt.2019.108710.

Neoh, Y.Y., Matanjun, P., Lee, J.S., 2016. Comparative study of drying methods on chemical constituents of Malaysian red seaweed. Dry. Technol. 34 (14), 1745–1751. https://doi.org/10.1080/07373937.2016.1212207.

Obluchinskaya, E., Daurtseva, A., 2020. Effects of air drying and freezing and long-term storage on phytochemical composition of brown seaweeds. J. Appl. Phycol. 32 (6), 4235–4249. https://doi.org/10.1007/s10811-020-02225-x.

Ong, S.P., Law, C.L., 2011. Drying kinetics and antioxidant phytochemicals retention of Salak fruit under different drying and pretreatment conditions. Dry. Technol. 29 (4), 429–441. https://doi.org/10.1080/07373937.2010.503332.

Peña-Rodríguez, A., Mawhinney, T.P., Ricque-Marie, D., Cruz-Suárez, L.E., 2011. Chemical composition of cultivated seaweed *Ulva clathrata* (Roth) C. Agardh. Food Chem. 129 (2), 491–498. https://doi.org/10.1016/j.foodchem.2011.04.104.

Ratti, C., 2001. Hot air and freeze-drying of high-value foods: a review. J. Food Eng. 49 (4), 311–319. https://doi.org/10.1016/S0260-8774(00)00228-4.

Ren, Z., Yu, X., Yagoub, A.E.A., Fakayode, O.A., Ma, H., Sun, Y., Zhou, C., 2021. Combinative effect of cutting orientation and drying techniques (hot air, vacuum, freeze and catalytic infrared drying) on the physicochemical properties of ginger (Zingiber officinale Roscoe). Lebensm. Wiss. Technol. 144, 111238 https://doi.org/10.1016/j.lwt.2021.111238.

Rojas, M.L., Augusto, P.E.D., 2018. Ethanol and ultrasound pre-treatments to improve infrared drying of potato slices. Innov. Food Sci. Emerg. 49, 65–75. https://doi.org/10.1016/j.ifset.2018.08.005.

Sánchez-García, F., Mirzayeva, A., Roldán, A., Castro, R., Palacios, V., G Barroso, C., Durán-Guerrero, E., 2021. Effect of different cooking methods on sea lettuce (*Ulva rigida*) volatile compounds and sensory properties. J. Sci. Food Agric. 101 (3), 970–980. https://doi.org/10.1002/jsfa.10705.

Stévant, P., Indergård, E., Ólafsdóttir, A., Marfaing, H., Larssen, W.E., Fleurence, J., Roleda, M.Y., Rustad, T., Slizyte, R., Nordtvedt, T.S., 2018. Effects of drying on the nutrient content and physico-chemical and sensory characteristics of the edible kelp *Saccharina latissima*. J. Appl. Phycol. 30 (4), 2587–2599. https://doi.org/10.1007/s10811-018-1451-0.

Tan, S., Ke, Z., Chai, D., Miao, Y., Luo, K., Li, W., 2021. Lycopene, polyphenols and antioxidant activities of three characteristic tomato cultivars subjected to two drying methods. Food Chem. 338, 128062 https://doi.org/10.1016/j.foodchem.2020.128062.

Uribe, E., Vega-Gálvez, A., García, V., Pastén, A., López, J., Goñi, G., 2019. Effect of different drying methods on phytochemical content and amino acid and fatty acid profiles of the green seaweed, *Ulva spp*. J. Appl. Phycol. 31 (3), 1967–1979. https://doi.org/10.1007/s10811-018-1686-9.

Vega-Gálvez, A., Miranda, M., Díaz, L.P., Lopez, L., Rodriguez, K., Di Scala, K., 2010. Effective moisture diffusivity determination and mathematical modelling of the drying curves of the olive-waste cake. Bio Technol. 101 (19), 7265–7270. https://doi.org/10.1016/j.biortech.2010.04.040.

Wu, J.N., Lin, C.H., Chen, X.T., Pan, N., Liu, Z., 2021. Polysaccharides isolated from *Bangia fuscopurpurea* induce apoptosis and autophagy in human ovarian cancer A2780 cells. Food Sci. Nutr. 9 (12), 6707–6719. https://doi.org/10.1002/fsn3.2621.

Wu, J., Chen, X., Chen, B., Pan, N., Qiao, K., Wu, G., Liu, Z., 2021. Collaborative analysis combining headspace-gas chromatography-ion mobility spectrometry (HS-GC-IMS) and intelligent (electronic) sensory systems to evaluate differences in the flavour of cultured pufferfish. Flavour Fragrance J. 36 (2), 182–189. https://doi.org/10.1002/ffj.3628.

Wu, J., Chen, X., Qiao, K., Su, Y., Liu, Z., 2021. Purification, structural elucidation, and in vitro antitumor effects of novel polysaccharides from *Bangia fuscopurpurea*. Food Sci. Hum. Wellness 10 (1), 63–71. https://doi.org/10.1016/j.fshw.2020.05.003.

Wu, Q., Fu, X.P., Sun, L.C., Zhang, Q., Liu, G., Cao, M., Cai, Q., 2015. Effects of physicochemical factors and in vitro gastrointestinal digestion on antioxidant activity of R-phycoerythrin from red algae *Bangia fusco-purpurea*. IJFST (Int. J. Food Sci. Technol.) 50 (6), 1445–1451. https://doi.org/10.1111/ijfs.12775.

Xu, Y.X., Jiang, Z.D., Du, X.P., Zheng, M.J., Fan-Yang, Y., Ni, H., Chen, F., 2022. The identification of biotransformation pathways for removing fishy malodor from *Bangia fusco-purpurea* using fermentation with Saccharomyces cerevisiae. Food Chem. 380, 132103 https://doi.org/10.1016/j.foodchem.2022.132103.

Xu, Y., Xiao, Y., Lagnika, C., Li, D., Liu, C., Jiang, N., Song, J., Zhang, M., 2020. A comparative evaluation of nutritional properties, antioxidant capacity and physical characteristics of cabbage (Brassica oleracea var. Capitate var L.) subjected to different drying methods. Food Chem. 309, 124935 https://doi.org/10.1016/j.foodchem.2019.06.002.

Yao, L., Liang, Y., Sun, M., Song, S., Wang, H., Dong, Z., Feng, T., Yue, H., 2022. Characteristic volatile fingerprints of three edible marine green algae (*Ulva spp.*) in China by HS-GC-IMS and evaluation of the antioxidant bioactivities. Food Res. Int. 162 (B), 112109 https://doi.org/10.1016/j.foodres.2022.112109.

Yu, D., Dong, L., Yan, F., Mu, H., Tang, B., Yang, X., Zeng, T., Zhou, Q., Gao, F., Wang, Z., Hao, Z., Kang, H., Zheng, Y., Huang, H., Wei, Y., Pan, W., Xu, Y., Zhu, J., Zhao, S., Li, H., 2019. eGPS 1.0: comprehensive software for multi-omic and evolutionary analyses. Natl. Sci. Rev. 6 (5), 867–869. https://doi.org/10.1093/nsr/nwz079.

Zhang, J., Cao, J., Pei, Z., Wei, P., Xiang, D., Cao, X., Shen, X., Li, C., 2019. Volatile flavour components and the mechanisms underlying their production in golden pompano (Trachinotus blochii) fillets subjected to different drying methods: a comparative study using an electronic nose, an electronic tongue and SDE-GC-MS. Food Res. Int. 123, 217–225. https://doi.org/10.1016/j.foodres.2019.04.069.

Zhang, L., Liao, L., Qiao, Y., Wang, C., Shi, D., An, K., Hu, J., 2020. Effects of ultrahigh pressure and ultrasound pretreatments on properties of strawberry chips prepared by vacuum-freeze drying. Food Chem. 303, 125386 https://doi.org/10.1016/j.foodchem.2019.125386.

Zheng, H.J., Zhang, S.Y., Guo, X., Lu, J., Dong, A., Deng, W., Tang, W., Zhao, M., Jin, T., 2014. An experimental study on the drying kinetics of lignite in high temperature nitrogen atmosphere. Fuel Process. Technol. 126, 259–265. https://doi.org/10.1016/j.fuproc.2014.05.009.

Zheng, M.J., Zheng, Y.J., Zhang, Y.F., Zhu, Y., Yang, Y., Oda, T., Ni, H., Jiang, Z., 2022. In vitro fermentation of *Bangia fusco-purpurea* polysaccharide by human gut microbiota and the protective effects of the resultant products on Caco-2 cells from lipopolysaccharide-induced injury. Int. J. Biol. Macromol. 222 (A), 818–829. https://doi.org/10.1016/j.ijbiomac.2022.09.217.